International Journal of Biological Macromolecules 194 (2022) 790–799

Contents lists available at ScienceDirect

International Journal of Biological Macromolecules

journal homepage: www.elsevier.com/locate/ijbiomac

Malachite Green, the hazardous materials that can bind to Apo-transferrin and change the iron transfer

Sadegh Farhadian [a,b,*], Fatemeh Hashemi-Shahraki [a,b], Sogand amirifar [a,b], Saeid Asadpour [c,**], Behzad Shareghi [a,b], Ehsan heidari [d], Behnam Shakerian [e], Mohammad Rafatifard [f], Ali Reza Firooz [g]

[a] Department of Biology, Faculty of Science, Shahrekord University, Shahrekord, P. O. Box.115, Iran
[b] Central Laboratory, Shahrekord University, Shahrekord, Iran
[c] Department of Chemistry, Faculty of Sciences, Shahrekord University, P. O. Box 115, Shahrekord, Iran
[d] Blood Transfusion Research Center, High Institute for Research and Education in Transfusion Medicine, Tehran, Iran
[e] Cardiovascular Diseases Research Department, Shahrekord University of Medical Sciences, Shahrekord, Iran
[f] Exercise Science/Physiology, Shahrekord University of Medical Sciences, Shahrekord, Iran
[g] Department of Chemistry, University of Isfahan, Isfahan, Iran

ARTICLE INFO

Keywords:
Malachite green oxalate
Apo-transferrin
Iron transfer
Multi-spectroscopy
Molecular dynamic simulation

ABSTRACT

Different groups of synthetic dyes might lead to environmental pollution. The binding affinity among hazardous materials with biomolecules necessitates a detailed understanding of their binding properties. Malachite Green might induce a change in the iron transfer by Apo-transferrin. Spectroscopic studies showed malachite green oxalate (MGO) could form the apo-transferrin-MGO complex and change the Accessible Surface Area (ASA) of the key amino acids for iron transfer. According to the ASA results the accessible surface area of Tyrosine, Aspartate, and Histidine of apo-transferrin significantly were changed, which can be considered as a convincing reason for changing the iron transfer. Moreover, based on the fluorescence data MGO could quench the fluorescence intensity of apo-transferrin in a static quenching mechanism. The experimental and Molecular Dynamic simulation results represented that the binding process led to micro environmental changes, around tryptophan residues and altered the tertiary structure of apo-transferrin. The Circular Dichroism (CD) spectra result represented a decrease in the amount of the α-Helix, as well as, increase in the β-sheet volumes of the apo-transferrin structure. Moreover, FTIR spectroscopy results showed a hypochromic shift in the peaks of amide I and II. Molecular docking and MD simulation confirmed all the computational findings.

1. Introduction

Cationic triarylmethane dyes are aromatic xenobiotic compounds commonly considered to be one of the main causes of environmental pollution [1,2]. Cationic triarylmethane dyes, including malachite green, have commonly been utilized in textiles, wool, acrylics, silk, leather, and paper industries due to their fungicide, disinfectant, and parasiticide properties, low cost, and widespread availability. These dyes are also used as additives and coloring in the food industry. Furthermore, because of their specific structure that can resist the transfusion-mediated transmission of certain human-related diseases, they have been used in the pharmaceutical industry [3–5]. However, cationic dye generally has a toxic and carcinogenesis effect. Contact with these pollutant compound cause mutation and even dermatological diseases. Therefore, dyestuff contaminants may create unfavorable situations. Also, they can cause negative impacts on living organism [6–8].

However, it has been reported malachite green oxalate had hazardous impacts on the various fish species and certain mammals. Because of their accumulation in the aquatic tissues, many countries have banned their use in the aquaculture of fish food [9,10]. Wastewater that contains synthetic colorants, the leftover dyes in water can cause significant damage to aquatic life due to their toxic feature [11–13]. Moreover, dyestuffs are not biodegradable because of their solubility specifications in the water [14]. Dyes are toxic even at a low concentration of less than

* Correspondence to: S. Farhadian, Department of Biology, Faculty of Science, Shahrekord University, Shahrekord, P. O. Box.115, Iran.
** Corresponding author.
E-mail addresses: farhadian@sku.ac.ir (S. Farhadian), s.asadpour@sku.ac.ir (S. Asadpour).

https://doi.org/10.1016/j.ijbiomac.2021.11.126
Received 30 October 2021; Received in revised form 16 November 2021; Accepted 17 November 2021
Available online 24 November 2021

1 ppm and are visible in the water [15]. In mammals, MGO might bring about organ damages, carcinogenic and mutagenic impacts, and developmental abnormalities, including the effects on the mammal reproduction of organisms, respiratory toxicity, and chromosomal abnormalities fractures [9,16,17]. Also, the presence of nitrogen in the structure of cationic triarylmethane dyes is a serious menace to human health and the aquatic environment [18,19]. In-vitro studies of MGO toxicity on the human tumor cell lines (HEp-2 and Caco-2) showed a remarkable reduction in cell proliferation. Despite the ban on their use, they are still illegally used in industries, especially the food industry, due to a lack of proper monitoring [20].

Moreover, the MG and its metabolite are toxic compounds with hazardous impacts on biological molecules. Recently researchers reported that MG has undesirable effects on the lipoprotein structure of the cell membrane and proteins structures. For instance, this dye interacted with HSA protein and caused structural changes by rising flexibility and reducing the HSA compactness. It also shifted the hemoglobin-specific structure to an inefficient form through the reduction content of α-helix and the increased content of random coil β-sheet, and β-turn [21]. Furthermore, the spectroscopic and molecular interaction between MG and lysozyme showed the instability effects on the protein [22]. Also, the interaction of MG with spectrin was investigated. Moreover, it was reported that the dye had distractive effects on this membrane skeletal protein [23].

Several studies reported MGO was found in the liver, kidney, muscles, serum, and other human organs. The prime site of transferrin synthesis is in the liver [9]. Therefore, MGO can directly interact with apo-transferrin and affect its function and lead to liver problems. It is well documented that apo-transferrin has a key role in iron transport through binding iron tightly and reversibly. Apo-transferrin causes iron transport by interactions of iron with two tyrosine, an aspartate, and histidine in the C-terminal and N-terminal of the protein and conformational changes that occur upon iron-binding. Therefore, MGO might potentially induce a change in the iron transfer by the protein [24–26].

Changes in the level of plasma transferrin are typically observed in those patients that suffer from iron deficiency anemia, atransferrinemia that results in heart failure as well several other related complications [27]. After entering MGO into the living organism body, the dye might attaché to apo-transferrin and effects the orientation of apo-transferrin to iron. Therefore, considering the importance of the mentioned contents, it seems that the study of the MGO interactions with apo-transferrin is critical. Accordingly, in the current study, MGO was chased as a synthetic dye, and apo-transferrin was picked as a protein pattern. The aim of this study was to highlight the biochemical effects of MGO on the structure and conformation of apo-transferrin. To our knowledge, we could eventually identify a novel pathway in the iron transport network at the apo-transferrin amino acids microenvironmental level. We also focused on spectroscopic techniques such as UV–Visible, fluorescence, circular dichroism, molecular dynamic simulations, and molecular docking for monitoring the effects of MGO on the protein structural and functional properties.

2. Materials and methods

2.1. Materials

Apo-transferrin (cod number: T1147, biological source: human, pH = 7.5, storage temperature: 4 °C), malachite green oxalate (cod number: C.I. 42,000, pH = 2.4 (24 °C, 10 g/L in H_2O) and Phosphate buffered saline (PBS) (solubility: doubly distilled water, pH = 7.5) were purchased from the company of Sigma Aldrich, USA. Apo-transferrin was dissolved in 0.05 M phosphate buffer and kept at 277 K. Apo-transferrin solution (0.1 $mg.ml^{-1}$) was prepared fresh for each assay.

2.2. Methods

2.2.1. UV–vis spectrophotometry

apo-transferrin UV–Vis spectra were monitored on a Pharmacia 4000 UV–Visible spectrophotometer from 200 to 350 nm. Apo-transferrin solution was titrated with different concentrations of malachite green oxalate (MGO) from 0 to 0.0025 mM. For monitoring the dye absorption spectrum overlapped with the apo-transferrin absorption spectral, to subtract MGO absorption effects at the maximum apo-transferrin wavelength, the dye with various levels of concentration was taken as the control sample that was, in turn, prepared without protein in the existence of various concentrations of MGO.

2.2.2. Fluorescence analyses

To examine the apo-transferrin tertiary structure, a Shimadzu RF-5301 fluorescence spectrophotometer was utilized. The wavelength values were recorded from 285 to 450 nm. The protein excited at the wavelength of 280 nm. The excitation and emission slits widths were 3.0 nm. 1.0 cm quartz cuvette was used for the assays. The concentration of apo-transferrin was kept at 0.1 mg/mL. The concentrations of the malachite green oxalate were from 0 to 0.0025 mM. To correct fluorescence emission spectra, the Internal Filtration Effect (IFE) was also taken into consideration by:

$$F_{corr} = F_{obs} \times e^{\frac{A_{ex}+A_{em}}{2}} \quad (1)$$

Where F_{obs} and F_{cor} were the observed and corrected fluorescence emission. A_{ex} indicated the absorption values of the sample at the excitation wavelength, and A_{em} related the absorption emission wavelength [28,29].

2.2.3. Circular dichroism spectroscopy

If an optically inactive biomolecule is placed in an asymmetric environment, like proteins, the behavior of circular dichroism (CD) would be altered for the native protein. When they interact with a ligand or pollutants, the conformational changes of these biomolecules can be evaluated [30]. Circular dichroism (CD) spectroscopy of apo-transferrin-MGO and native apo-transferrin were studied with the Spectropolarimeter model 215 equipped by 1 mm diameter cuvette at 298 K. The obtained results were recorded from 200 to 260 nm range. The concentration solution of apo-transferrin was kept at 0.1 mg/mL. The CDNN [31,32] was also applied to investigate the secondary structure elements of the protein.

2.2.4. Molecular docking

To anticipate the dominant binding modes of a compound with a protein via a known 3D structure, molecular docking is a crucial tool [33]. The molecular docking assays between apo-transferrin and MGO were done by the Auto dock 4.2.1 program [34]. Apo-transferrin 3D structure with PDB ID 2hav was driven from the RCSB-PDB (http://www.rcsb.org/pdb). PubChem site was applied to obtain the molecular structure of the MGO and optimized by the chimera ucsf [35,36]. Obtained protein and ligand structure saved in PDB format. Over the assay, malachite green oxalate was considered flexible and apo-transferrin was rigid. Molecular docking was done in two stages, the first stage for determining the stereochemical form of the compound and the final stage to find the interaction mood and select the best stereochemical compound and protein configuration. During molecular docking analyses, some factors like orientation and random torsion were investigated for MGO. The grid box size of the apo-transferrin-MGO system, with the 1A° spacing, was 126 Å × 126 Å × 126 Å. In the current system, all essential hydrogen atoms were added to apo-transferrin with a grid spacing of 1 Å. To evaluate the intermolecular interactions, chimera software and R-studio discovery (version V 16.1) were applied [37].

2.2.5. Molecular dynamic (MD) trajectory

To analysis the MD trajectory of apo-transferrin and MGO, the Gromacs 5.7.1 program was applied [38]. There were some important parameters during MD trajectory, including Force field (for numbering apo-transferrin and water): amber 99, Box size: 6.701 Å × 6.701 Å × 4.738 Å, Number of water molecules: 52744, Water model: Tip4p, the steps number 60000000, Time-step: 1 fs, Ion: 3 Na^+, Total charge: −3, Temperature: 300 K. Brendes algorithm was used to equilibrate the water around the apo-transferrin and energy minimization. The time of simulation was 60 ns.

2.2.6. Fourier-transform infrared (FTIR) spectroscopy

The Fourier Transform Infrared (FTIR) spectra (ATR accessory) of apo-transferrin and apo-transferrin-MGO were used to characterize the secondary structure alteration after complex formation (Perkin Elmer – two spectrums, USA). The spectra were recorded in the range of 1500 to 1750 cm^{-1}.

3. Results and discussion

3.1. Absorption spectroscopy

UV–Vis spectroscopy is typically utilized for the quantitative determination of varying analytics, involving highly conjugated organic compounds, transition metal ions, and biological macromolecules [39–44]. This technique is an efficient way to evaluate the complex formation between a compound with a protein. The interaction between a ligand with a biomolecule is accompanied by a hyperchromic or hypochromic effect [45]. If the UV–Vis spectra are almost fixed, the hyperchromic effects would be observed. Hypochromic effects were accrued in cases that the alter in the peptide backbone conformation connected with the Helix- coil transformation [46]. The complex formation between a compound and protein caused alterations in the absorption spectra. When UV–Vis absorption spectra change, the quenching mechanism is static, but if the absorption spectrum does not alter the quenching mechanism would be a dynamic one [47]. The formation of an absorption peak at 280 nm has resulted from $\pi \rightarrow \pi^*$ electron transition in some chromophores such as Trp and Tyr residue [48]. Apo-transferrin configuration variations were monitored using absorption spectroscopy. The UV–Vis spectra of the MGO 's interaction with apo-transferrin have been shown in Fig. 1. As observed, the increases of the absorption spectra (hyperchromic effects) at the range of 280 nm resulted from the rising concentration of MGO. The alteration in the percentage of the apo-transferrin absorption showed the complexation between the protein and ligand. According to the absorption spectra, it appears that the static quenching mood is more likely. As a result, the interaction between the dye with apo-transferrin could shift the hydrophobicity of the protein. To accomplish the correct results, the absorption intensity of the dye sample was deducted from the apo-transferrin-MGO complex due to the dye had absorption at a wavelength in the range close to that of the apo-transferrin absorption.

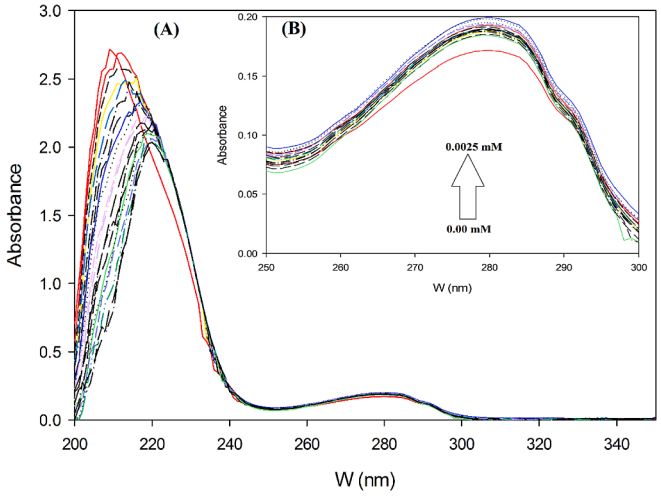

Fig. 1. (A): The UV absorption of apo-transferrin (0.1 $mg.ml^{-1}$) in the presence of MGO (0.0–0.0025 mM) at pH 7.5 and 298 K, and (B): Absorbance peak at 280 nm region versus difference concentration of MGO.

3.2. Fluorescence quenching measurements

In fluorescence spectroscopy, first, a molecule is excited via the absorption of a photon. After that, it reaches one of the different vibrational states in the electronically excited state [49–52]. As a result of a collision with other compounds, the excited molecule loses its vibration energy to the point that it has the least vibration state from the excited electronic state. Thus fluorescence is the result of the excitation of the ground state and emission spectra in a molecule containing inner intrinsic fluorophores groups including tryptophan (Trp), tyrosine (Tyr), and phenylalanine (Phe) [53]. The microenvironment of the Trp residues is completely sensitive to the changes, so these properties could be the best option to evaluate the protein conformational change [54]. There are 8 tryptophan amino acids in the apo-transferrin that act as the main intrinsic fluorophores and have critical roles in the intrinsic emission of fluorescence [55]. The interaction between apo-transferrin and MGO at 308, 318, 328 K temperature and 331 nm *wavelength* was done using fluorescence evaluation. The alteration in the intrinsic fluorescence emission could reveal the formation of the apo-transferrin-MGO complex obtained as a result of the modifications in the fluorophore microenvironment of the protein. Various compounds with different quenching processes might alter the internal emission fluorescence of the protein. The fluorescence emission spectra of the free protein and complex form with MGO, at three different temperatures, in the excited mood at 280 nm, have been shown in Fig. 2 (A–F). In the current analysis, the MGO concentrations were selected as there was no apparent overlap of self-absorption and spectral (0.0–0.0025 mM). Evaluation of the fluorescence spectra discovered that the intensity of emission reduced up to ~32% by regularly increasing the concentration of the MGO. Reduction of the fluorescence intensity is related to many interactions with the donor molecule, including excitation of the ground-state, ligand blackout collision, ground-state complexation, molecular rearrangements, and energy transfer [56]. When the MGO is absent, the emission spectra of apo-transferrin were detected at 357.23 nm. Apo-transferrin emission spectra changed to shorter wavelengths, by joining the MGO to 240.19 nm. The hypo-shifts in the emission intensity of apo-transferrin with increasing concentration of the MGO represent the increased toxicity to the protein at more concentration levels of the pollutant. Generally, hypo shift in the emission peak resulted from two main reasons: I) change in the hydrophilicity microenvironment of the aromatics residues, and II) placed these chromophores near a charged group. The hypo-shift effects induced by MGO could drive from the tryptophan residues exposure to a more hydrophilic region, representing the tertiary structural change in the apo-transferrin.

3.3. Apo-transferrin quenching mechanisms

There are three kinds of protein fluorescence quenching mechanisms induced by ligand: static quenching, dynamic quenching, and mixed form. Static quenching accrued as a result of the ground–state complexation [57]. Dynamic quenching has been driven from the collision between fluorophore (apo-transferrin) and quenchers (MGO). The mixed quenching results from the combination of dynamic and static quenching [58,59]. With joined MGO to the protein solution, fluorescence quenching accrued. The apo-transferrin fluorescence quenching mood in the presence of MGO was evaluated as a static quenching mechanism. Quantitative analyses of the apo-transferrin

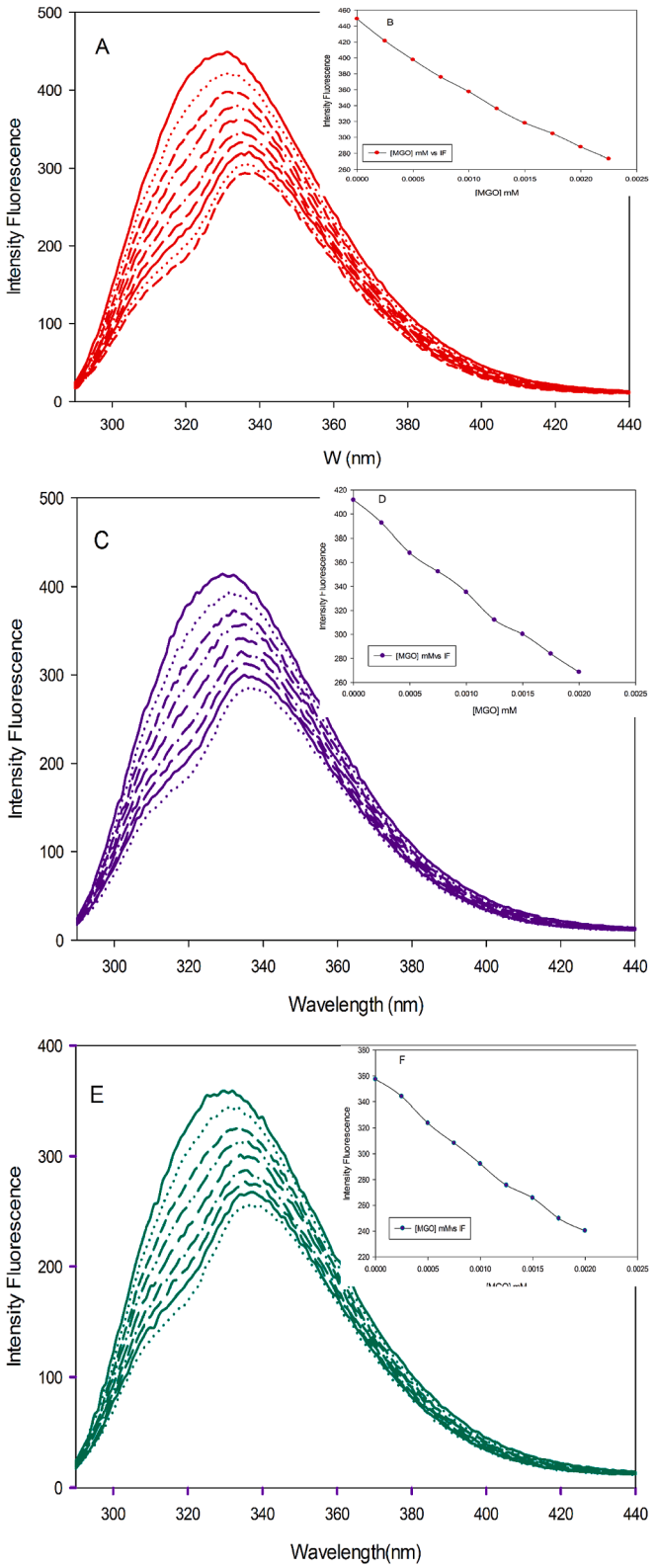

Fig. 2. Apo-transferrin emission spectrum (0.1 mg.ml^{-1}) with and without MGO at pH 7.5 and 308 K (A), 318 K (C), and 328 K (E). Fluorescence emission intensity at 331 nm against the various amount of MGO (B, D, and F).

fluorescence quenching mechanism induced by MGO were studied by the equation of Stern–Volmer [60–64]:

$$\frac{F^0}{F} = 1 + K_{SV}[Q] = 1 + k_q\tau_0[Q] \quad (2)$$

F^0 = free apo-transferrin Fluorescence intensity
F = quencher (MGO) Fluorescence intensity
[Q] = MGO Concentration
K_{SV} = Stern-Volmer quenching constant
k_q = Quenching rate constant
τ_0 = The mean lifetime of apo-transferrin with no quencher (10^{-8} s)

The Stern-Volmer diagram was plotted in Fig. 3. It represented the quenching emission spectra of the apo-transferrin-MGO complex. According to Table 1, raising temperature reduced protein K_{SV} amounts. Quantitative rates of K_{SV} were calculated by considering the slope of the apo-transferrin -MGO complex diagram. The values of the quenching constant, K_q, obtained by the following equation [65,66]:

$$K_{sv} = k_q\tau_0 \quad (3)$$

K_{SV} = Stern-Volmer quenching constant
K_q = quenching constant
τ_0 = The mean lifetime of the protein with no quencher

In cases where the value of K_q is higher than 2×10^{10} L mol^{-1} s^{-1}, the mechanism of quenching results from the complexation of the ground-state [67]. As listed in Table 1 the quantitative values of K_q were more than 2.0×10^{10} mol^{-1} s^{-1}. According to Fig. 5, a linear relationship was obvious between the initial and secondary fluorescence emission with the concentration of MGO. Also, the quantitative values of the Stern-Volmer constant reduced with rising temperature. Based on the above data, the quenching mechanism was considered as static type, by calculating the quenching constant. With computational approaches and data analysis, it concluded that the quenching events were a result of forming the non-fluorescent complex.

3.4. Apo-transferrin-MGO binding constant and number of binding

Based on the obtained data from the static quenching mechanism of apo-transferrin induced by MGO, the binding parameters such as the binding site MGO number (n) on the protein and apparent binding constant (K_a) were calculated using Eq. (4) [67–70]:

$$log(F0\_F)/F = \log k_{binding} + n\log[Q] \quad (4)$$

F0 = the apo-transferrin Fluorescence intensity
F = the apo-transferrin-MGO Fluorescence intensity
$k_{binding}$ = Binding constant
n = binding sites number

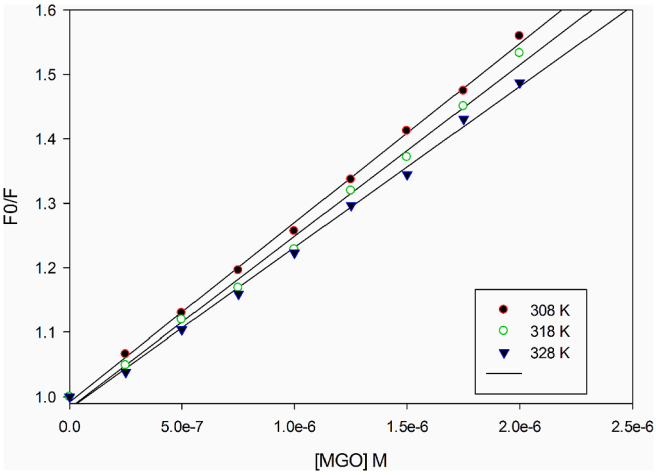

Fig. 3. Stern Volmer plot for the interaction of MGO with apo-transferrin at different temperatures: 308, 318, and 328 K.

Table 1
Stern–Volmer quenching constants of the apo-transferrin-MGO complex at three temperatures.

T (K)	$K_{sv} \times 10^3 (M^{-1})$	K_q ($10^{12} M^{-1} S^{-1}$)	R^2
308	285.94 ± 1.7	28.59 ± 0.17	0.99
318	273.72 ± 5.6	27.37 ± 0.56	0.99
328	259.23 ± 6.4	25.92 ± 0.64	0.99

The MGO number of binding sites (*n*) per apo-transferrin molecule and MGO binding constant (K_b) were computed using diagraming log [(F_0 − F)/F] against log [Q]. The Stern–Volmer logarithm diagram related to the effect of MGO on the apo-transferrin has been shown in Fig. 4. Examination of the Stern–Volmer plot showed a linear correlation between F0/F and the MGO concentrations. In this plot, the slope was equal to K_{SV}. It is well known the binding constant is a temperature-dependent parameter. According to the driven results, accompanied by raising the temperature, the binding sites MGO number (n) on the apo-transferrin and binding constant (K_b) were decreased. These results discovered that the binding of MGO on the apo-transferrin was an exothermic process, also accompanied by raising the temperature, MGO binding capacity was reduced. The fluorescence estimated binding constant was in good agreement with the UV–Vis estimations.

3.5. Apo-transferrin thermodynamic parameters

To assess the kind of interaction forces between malachite green oxalate and apo-transferrin, thermodynamic parameters must be determined as a function of temperature. Non-covalent intermolecular interactions including hydrophobic bonds, Van der Waals forces, electrostatic interactions, and hydrogen bonds are of great importance in the ligand binding to proteins. During the temperature range, in cases where the enthalpy (ΔH°) changes are small, the thermodynamic factors such as ΔS°, and ΔG° can be calculated using the equation of Van't Hoff. The equation is applied to estimate the changes in the entropy, enthalpy, and total energy [71,72].

$$lnKa = -\frac{\Delta H^\circ}{RT} + \frac{\Delta S^\circ}{R} \quad (5)$$

K_a = Binding constant
ΔH° = Standard enthalpy
ΔS° = Standard entropy
T = temperature
R = universal gas constant

$$\Delta G_{bindi}ng^0 = -RTlnk_{binding} \quad (6)$$

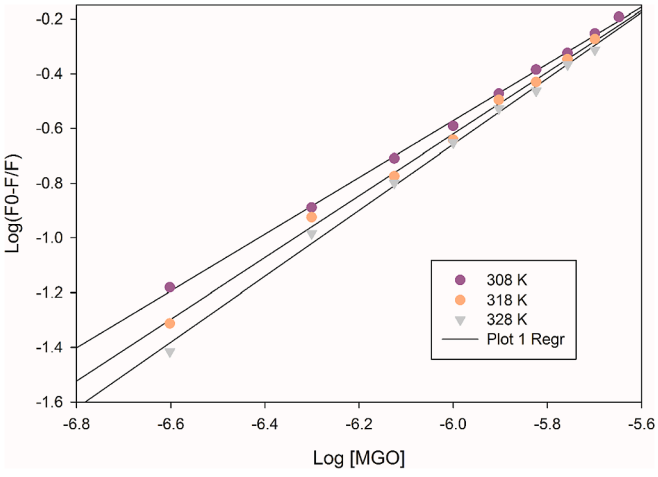

Fig. 4. Stern–Volmer logarithm diagram related to MGO interaction with apo-transferrin at three temperatures.

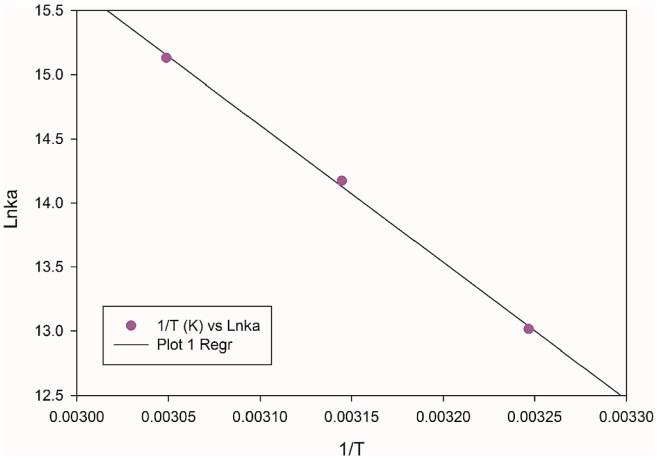

Fig. 5. The Ln K vs. log 1/T plot of the apo-transferrin-MGO complex at different temperatures.

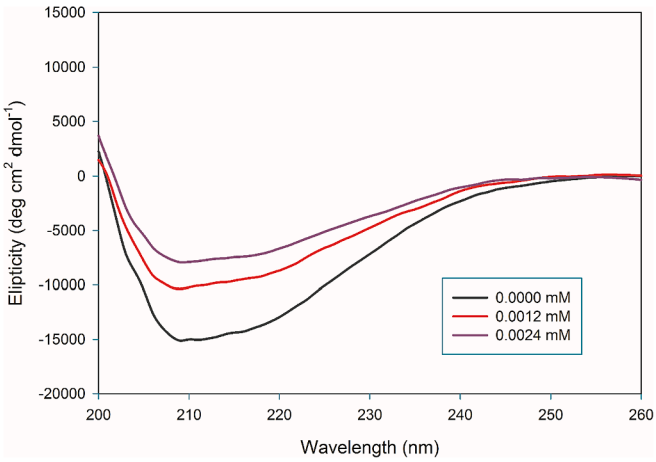

Fig. 6. The secondary structure plot of apo-transferrin with and without MGO.

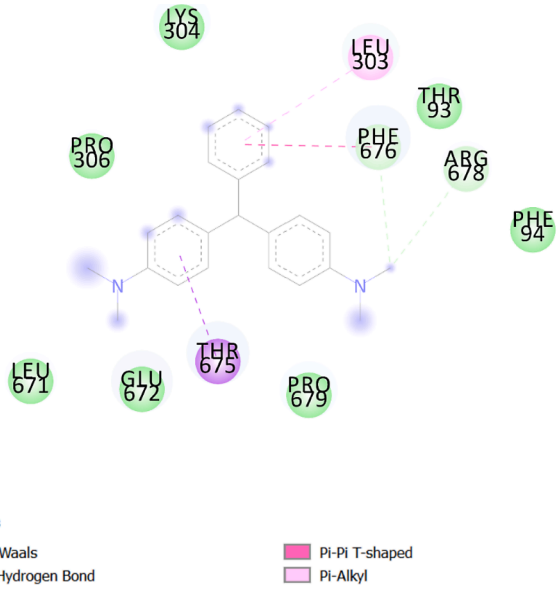

Fig. 7. Auto Dock diagram of the native and complex form of apo-transferrin with MGO.

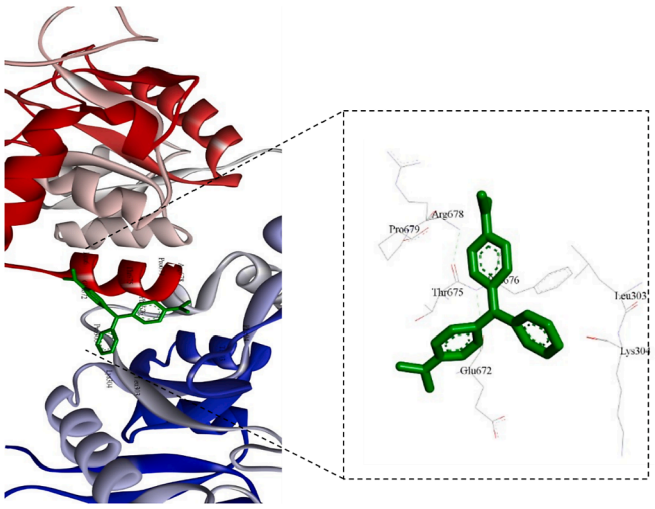

Fig. 8. The secondary structure of docked MGO and apo-transferrin.

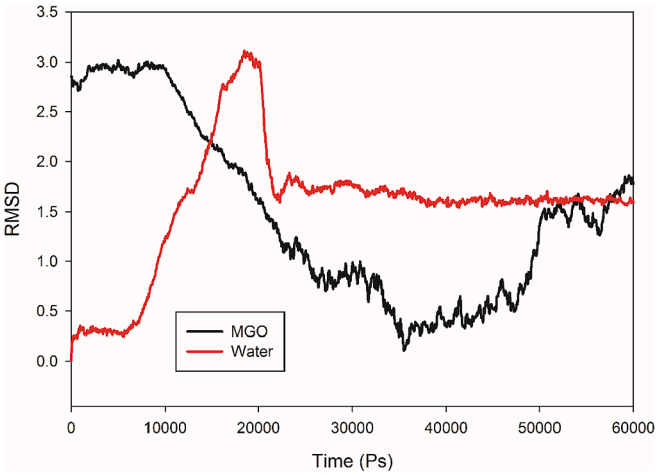

Fig. 9. Root mean square deviation (RMSD) of native apo-transferrin and apo-transferrin-MGO complex.

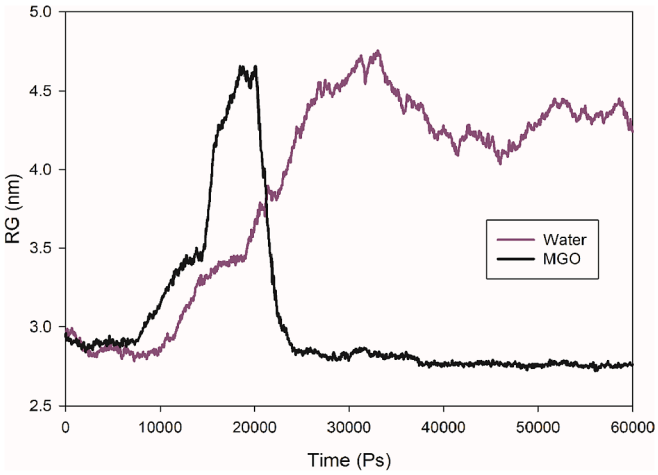

Fig. 10. Gyration radius of native apo-transferrin and apo-transferrin-MGO complex.

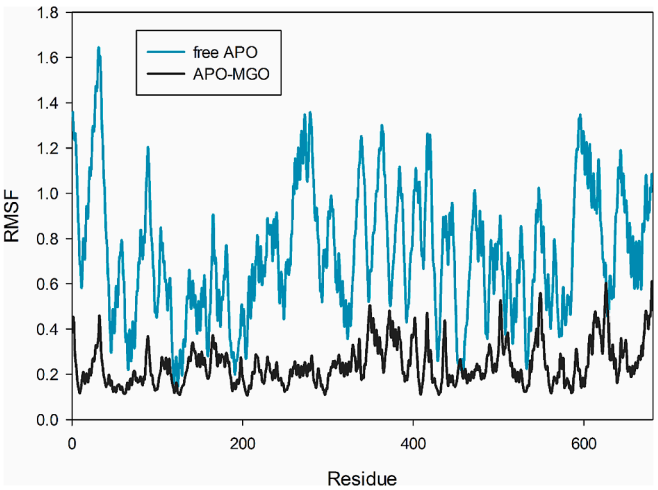

Fig. 11. Root mean square fluctuation (RMSF) of native apo-transferrin and apo-transferrin-MGO complex.

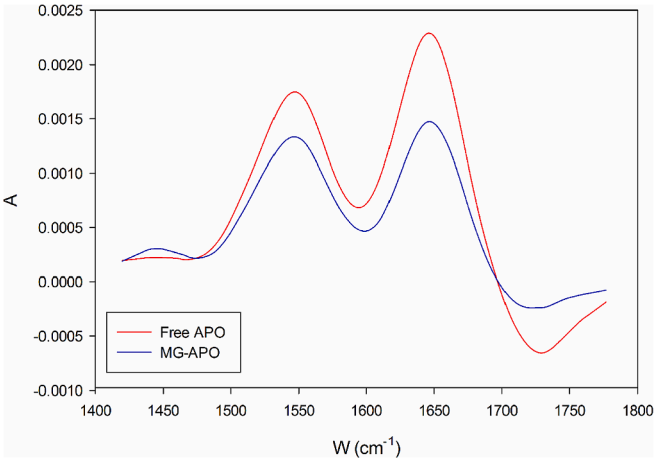

Fig. 12. Background FTIR spectrum of the free apo-transferrin (A) and apo-transferrin -Malachite green oxalate complex. (For interpretation of the references to colour in this figure legend, the reader is referred to the web version of this article.)

$\Delta G^0_{binding}$ = Standard binding free energy.
$k_{binding}$ = Binding constant

$$\Delta S^\circ = \frac{\Delta H^\circ - \Delta G^\circ}{T} \quad (7)$$

$$\Delta G^\circ = \Delta H - T\Delta S = -RTlnK \quad (8)$$

The intermolecular forces can be determined by calculating the quantitative values of Gibbs free energy, enthalpy, and entropy parameters [67]. By determining the values of enthalpy and entropy type of non-covalent forces between MGO and apo-transferrin can be determined this. The free energy change (ΔG) in the current interaction was calculated using Eq. (8). Ross and et al. in 1980 reported the specifications thermodynamic parameters of the ligand-protein interaction. Based upon their thermodynamic results-driven from large molecule model systems, the positive quantitative values of entropy and enthalpy represented the hydrophobic association. In contrast, their negative values are indicative of hydrogen bonds and Van der Waals forces. In cases where the enthalpy is negative or slight positive and the entropy is positive, the dominant interaction force between ligand and protein is considered electrostatic (ionic). According to the positive values of the ΔH and ΔS, dominant forces between MGO and apo-transferrin were

Table 2
Thermodynamic parameters of the apo-transferrin-MGO complex at pH 7.5 and three temperatures.

T (K)	$K_a \times 10^4$ (M^{-1})	*n*	R^2	ΔH° (kJ mol^{-1})	ΔS° (J mol^{-1} K^{-1})	ΔG° (kJ mol^{-1})
308	55.62 ± 9.2	1.06 ± 0.02	0.99	73.58 ± 15.59	372.31 ± 26	−34.15 ± 0.71
318	132.59 ± 20.8	1.12 ± 0.02	0.99			−37.58 ± 0.75
328	305.96 ± 81.6	1.19 ± 0.03	0.99			−41.6 ± 0.91

Van der Waals interactions. The thermodynamic parameters have been reported in Table 2. Driven results revealed a good harmony between the obtained $\Delta G^0_{binding}$ values and the extrapolated free binding energy resulting from the molecular docking studies.

3.6. Circular dichroism measurement

Circular Dichroism (CD) is absorption spectroscopy used to study the secondary structure properties of optically active molecules [73]. Far-CD spectroscopy is mostly regarded to study biomolecules, their structure, and interactions with a ligand or other molecules. There are many advantages of using this technique including simple analysis, low volume samples, no destructiveness, and accuracy results [74,75]. The content of apo-transferrin secondary structures in the absence and presence of MGO was recorded from 200 nm to 260 nm which was evaluated by the CDNN software [76]. The alteration in the secondary structure elements of apo-transferrin accompanied with MGO is reported in Fig. 6 and Table 3. Apo-transferrin contains β-sheet and α-Helix structure. With the addition of MGO, the alteration of secondary structures was observed. In the existence of MGO, the percentage of β-sheet increased, while the content structure of the α-helix was decreased. The increased content of β-sheet caused disorderly structure in association with MGO. Far-UV CD results were represented the apo-transferrin secondary structural changes in the presence of MGO. The CD results were in good accordance with the result of fluorescence spectroscopy. For more accuracy of these data, molecular dynamic simulation was carried out that the obtained results appropriately accord with those of CD and fluorescence spectroscopy.

3.7. Molecular dynamic (MD) simulations

3.7.1. Molecular docking studies

Experimental tests upon molecular docking studies are the most accurate method to evaluate the interaction between ligand and protein in atomic details, accurate identification of the interaction of binding, and determining the ligand-binding site on the protein by estimating the free energy of binding [77]. Auto Dock 4.2.1 software was also employed to evaluate the interaction between MGO and apo-transferrin for monitoring the binding site, position of the conformational changes, and type of interactions [78]. The best binding site of the dye on the apo-transferrin has been shown in Fig. 7. All calculated energy and binding energies between the pollutant and protein were listed in Table 4. Therefore, the complex formation was a spontaneous reaction. Fig. 8 represented the type of interactions. The Van der Waals interactions were dominant forces between MGO and apo-transferrin. As observed, intramolecular interactions were between MGO and Arg678, Phe676.

Table 3
The secondary structures of the apo-transferrin.

[MGO]	α-Helix (%)	β-Sheet (%)	β-Turn (%)	Random Coil (%)
0.0000 mM	43.86	13.61	16.21	26.29
0.0012 mM	29.20	19.50	17.62	33.66
0.0024 mM	23.69	21.89	17.72	36.68

Table 4
Docked data with interacting amino acids after 200 runs.

Estimated Free Energy Binding (KCal/mol)	Estimated Inhibition Constant, (KCal/mol)	Final Intermolecular Energy (KCal/mol)	VdW + Hbond+ Desolv Energy (KCal/mol)	Final Total internal Energy (KCal/mol)	Torsional free Energy (KCal/mol)
−4.28	734.75	−5.77	−5.76	−1.11	+1.49

Also, pi binding was formed with Phe676, Leu303, and Thr675. Since the pollutant was surrounded by the protein, MGO embedded in the apo-transferrin secondary structure induced more adverse effects on the protein structure and activity. According to the molecular docking studies, the MGO might bind to the protein, which, in turn, was in perfect harmony with the results of UV–Vis, fluorescence, and CD spectroscopy.

3.8. Molecular dynamic simulation

3.8.1. Apo-transferrin conformation

Molecular dynamic (MD) simulation can supply valuable reports about the atoms and molecules to study the protein conformational changes, stability, and flexibility in the existence of a ligand [79–82]. Numerous factors including root mean square fluctuation (RMSF), gyration radius (RG), and accessible surface area (ASA) are typically involved in evaluating the presses of the protein interaction with a ligand [83]. In the molecular dynamic simulation, estimation of the Root Mean Square Deviations (RMSDs) is a precise technique for examination of the protein structural and conformational properties, average distances between the amino acid residues of protein with a ligand, and protein stability [84,85]. Apo-transferrin structural properties were evaluated in the existence of MGO by RMSD. The RMSD of apo-transferrin and complex form with MGO has been shown in Fig. 9 and Table 5. The RMSD of apo-transferrin in comparison with the apo-transferrin-water system increased when MGO was present. It could be considered that MGO has continuously interacted with apo-transferrin and finally caused the un-stability of the protein.

To obtain data on the apo-transferrin conformation and structural compactness during the MD simulation, the protein gyration radius (RG) was studied. Protein gyration radius is a type of Rg providing valuable information on the correlation of protein condensation and protein folding [86]. The RG result of the apo-transferrin and its structural alterations in the presence of the pollutant have been presented in Fig 10. In the apo-transferrin-MGO complex, the values of RG were less than the native protein that means increasing the amount of the apo-transferrin stability led to raising protein compression. Also, the amounts of hydrogen bonds protein-protein were increased but the amounts of hydrogen bonds protein-water decreased. These results indicated an increase in protein compression. The RMSD and RG results, accompanied with the obtained data on the changed values of apo-transferrin α-helix and β-sheet from CD spectroscopy has suggested an increase in the protein compactness. The RMSD and RG results were confirmed the driven results of the CD studies.

3.8.2. Apo-transferrin flexibility

In cases a system is flexible in some locations; the average flexibility in the biomolecule can be calculated during the simulation analysis. The Roots Mean Square Fluctuation (RMSF) presents the average flexibility in the biomolecule over the simulation [87,88]. The RMSF parameter was applied to monitor the conformational flexibility of apo-transferrin in the existence and inexistence of MGO. RMSF plot of a native and complex form of apo-transferrin with MGO has been shown in Fig. 11. The RMSF of apo-transferrin decreased in the existence of MGO, which represents this system had less flexibility over the simulation. Hence,

Table 5
The average and standard deviations of MD simulation parameters.

Protein	RMSD (nm)	RG (nm)	RMSF (nm)	Hydrogen bonds protein-protein	Hydrogen bonds protein-water	SASA (nm)
apo-transferrin	1.54 ± 0.14	4.36 ± 0.04	0.72 ± 0.28	469.86 ± 11.31	1234.33 ± 22.04	370.79 ± 2.06
apo-transferrin-MGO complex	1.61 ± 0.02	2.75 ± 0.01	0.24 ± 0.09	497.42 ± 11.90	1182.81 ± 22.48	370.09 ± 2.03

adding MGO reduced the residues dynamic, and the protein changed into a tight form. The results related to MD simulations complied with those of the Far-UV CD spectroscopy. All these results revealed an increase in the content of the β-sheet elements. The increase in the content of β-sheet caused a disorganized form in the apo-transferrin structure.

3.8.3. Apo-transferrin secondary structure analysis

To more confirm the secondary structure alteration results driven from the experimental studies, the MD simulation was considered [89]. The amounts of amino acids extant in the secondary structure of apo-transferrin have been shown in Fig. 12 and Table 6. This plot showed the amino acids level residues in the secondary structure of apo-transferrin in the free form and complex with MGO. The obtained data from the MD simulation the scout file. The driven results from the scout file might be used to monitor the amino acids participation level in the apo-transferrin secondary structure. According to the Table 3, the percentage of β-sheet was increased while the α-Helix was decreased which was in good harmony with the CD spectroscopy results. These results represented that MGO was bonded to apo-transferrin and this interaction leads to some changes in the secondary structures of the protein. Apo-transferrin secondary structure analysis in the MD simulation showed the protein had become less flexible. Moreover, an increase in the apo-transferrin compactness was observed (decreasing in RG values). Hence, apo-transferrin in the complicated form with MGO has been less able to carry Fe^{2+} and other compounds in the storm of blood. As mentioned in the introduction part, a defective connection with iron could cause heart failure and many other malfunctions.

3.8.4. Accessible surface area for important amino acids of Apo-transferrin

To better understand the location and alteration of the residues, the Accessible Surface Area (ASA) of amino acids was done for the free and complex form of apo-transferrin with MGO [90]. The changes in the ASA according to the binding of MGO to the apo-transferrin were studied. As mentioned, apo-transferrin coordinates iron through interactions with two Tyr, an Asp, and a His in both C-terminal and N-terminal domains of apo-transferrin and also conformational changes that occur upon iron-binding. Induces any change in the accessible surface area of these amino acids can alter the orientation of apo-transferrin to iron. The ASA results were presented in Table 7. Based on the results, the ASA values of the Tyr92, Tyr426, Asp63, His249, significantly increased which represents a shift to a more external position. Moreover, the SASA values of the Tyr95, Tyr188, Tyr517, Asp392, His585, Trp8, Trp128, Trp358, Trp460, and Trp550 residues decreased. Therefore, these residues shifted to a more internal position in the presence of MGO. The binding of MGO to the apo-transferrin caused engraved the location of these residues to a less polarized microenvironment, which lead to an increase in compactness of the apo-transferrin structure, and significantly changed its orientation to iron. This result can be considered a change in iron transport.

Table 7
ASA for the residues for free pepsin and apo-transferrin **–MGO** complex.

Residue	Water	MGO	ΔASA l-w	%
Tyr95	0.629	0.622	−0.007	−1.11
Tyr188	0.556	0.535	−0.021	−3.77
Tyr426	0.644	0.657	0.013	2.01
Tyr517	0.570	0.537	−0.033	−5.78
Asp392	0.556	0.484	−0.072	−0.12.94
Asp63	0.504	0.538	0.034	6.74
His585	0.513	0.445	−0.068	−13.25
His249	0.445	0.512	0.067	15.05
Trp8	0.449	0.435	−0.014	−3.11
Trp128	0.571	0.496	−0.075	−0.013
Trp264	0.555	0.562	0.007	1.26
Trp344	0.456	0.464	0.008	1.75
Trp358	0.515	0.384	−0.131	−25.43
Trp441	0.504	0.639	0.135	26.78
Trp460	0.470	0.444	−0.026	−5.53
Trp550	0.622	0.601	−0.021	−3.37

3.9. Fourier transform infrared spectra

The secondary structure of apo-transferrin in the presence of MGO was studied using FTIR spectroscopy. The relative intensity of IR bands for apo-transferrin is between 1700 and 1600 cm^{-1} (C═O stretch) and between 1600 and 1500 cm^{-1} (C—N stretch coupled with N—H bending). The sensitivity of the amide I band was normally utilized to explain the change of secondary structures in proteins [82]. The amide I band between 1600 and 1700 cm^{-1} found in our study is mainly due to the C═O stretch of peptide linkages (approximately 80% of the potential energy) and is directly related to the backbone conformation; amide I is also the most sensitive spectral region. Amide II, at approximately 1600–1450 cm^{-1}, results from the N—H bending (40–60% of the potential energy) and the C—N stretching (18–40%); this band is conformational sensitive [91]. In Fig. 12, a hypochromic shift was observed in the peaks of amide I and II. In apo-transferrin, a conformational shift and redistribution of the helical structure can be seen. Meanwhile, due to the interaction of MGO with the C═O and C—N groups of protein polypeptides, there was a reduction in the intensity of the amide I band when MGO was added. The results from the FTIR and CD were found to be in agreement.

4. Conclusion

In the recent study, the binding interaction between MGO and apo-transferrin was studied by using various spectroscopic methods. The obtained results from spectroscopy methods and molecular dynamic simulation discovered that MGO could induce change in the apo-transferrin native conformation and structural properties. MGO caused quench the intrinsic fluorescence of apo-transferrin by 33% in a static quenching mechanism. Obtained values of binding constant ($k_{binding}$) for

Table 6
Secondary structure content of the native and complex form of apo-transferrin.

Protein	α-Helix (%)	β-sheet	3-Helix	β-Bridge (%)	β-Turn (%)	Random Coil (%)	Bend (%)
apo-transferrin	186.40 ± 5.77	112.10 ± 5.95	13.05 ± 4.99	122.19 ± 6.26	80.13 ± 8.78	152.72 ± 5.99	122.19 ± 6.26
apo-transferrin **–MGO complex**	187.25 ± 4.10	117.71 ± 5.7	14.5 ± 4.7	5.29 ± 2.61	81.31 ± 6.88	146.65 ± 5.64	121.33 ± 6.25

the apo-transferrin-MGO complex, showed a high-affinity connection between the dye and apo-transferrin. Moreover, MGO reduced hydrogen bonding networks decreased the flexibility of the protein by reducing the content of α-Helix and increasing the contents of β-sheet and β-turn. According to the obtained experimental and computational data, we found that MGO, as a synthetic dye and a pollutant factor, could bind to apo-transferrin and significantly alter the accessible surface area of key amino acids of apo-transferrin for iron-binding with a high affinity. Apo-transferrin has undergone the conformational changes that occur upon MGO binding. Therefore, MGO can be considered as a factor to change the orientation of apo-transferrin to iron, and thus it might potentially trigger change in the iron transfer by the protein. The dye caused completely wasted bioactivity of the protein. Finally, we could identify a novel pathway in the iron transport network at the apo-transferrin amino acids microenvironmental level.

References

[1] G. Singh, T. Koerner, J.-M. Gelinas, M. Abbott, B. Brady, A.-C. Huet, C. Charlier, P. Delahaut, S. Benrejeb Godefroy, Food Addit. Contam. 28 (2011) 731–739.
[2] G. Karthigadevi, S. Manikandan, N. Karmegam, R. Subbaiya, S. Chozhavendhan, R. Balasubramani, S.W. Chang, M.K. Awasthi, Bioresour. Technol. 324 (2021), 124678.
[3] W. Huang, H. Yang, S. Zhang, J. Hazard. Mater. 366 (2019) 520–528.
[4] Ö. Tacal, I. Özer, J. Biochem. Mol. Toxicol. 18 (2004) 253–256.
[5] C.R. White, S.J. Davies, T.B. Henry, Zebrafish 9 (2012) 135–139.
[6] E. Altıntıg, H. Altundag, M. Tuzen, A. Sarı, Chem. Eng. Res. Des. 122 (2017) 151–163.
[7] E. Altintig, M. Onaran, A. Sarı, H. Altundag, M. Tuzen, Mater. Chem. Phys. 220 (2018) 313–321.
[8] M. Tuzen, A. Sarı, T.A. Saleh, J. Environ. Manag. 206 (2018) 170–177.
[9] S. Srivastava, R. Sinha, D. Roy, Aquat. Toxicol. 66 (2004) 319–329.
[10] E. Sudova, J. Machova, Z. Svobodova, T. Vesely, Veterinarni Medicina-Praha- 52 (2007) 527.
[11] M. Srinivas, R.C. Venkata, R.R. Kakarla, N.P. Shetti, M. Reddy, V.R. Anjanapura, Mater. Res. Express 6 (2019), 125502.
[12] U. Jinendra, D. Bilehal, B. Nagabhushana, K.R. Reddy, C.V. Reddy, A.V. Raghu, Mater.Sci.Energy Technol. 2 (2019) 657–666.
[13] U. Jinendra, J. Kumar, B. Nagabhushana, A.V. Raghu, D. Bilehal, Green Mater. 7 (2019) 137–142.
[14] E. Altıntıg, M. Yenigun, A. Sarı, H. Altundag, M. Tuzen, T.A. Saleh, Environ. Technol.Innov. 21 (2021), 101305.
[15] T.A. Saleh, S.H. Al-Ruwayshid, A. Sarı, M. Tuzen, Eur. Polym. J. 130 (2020), 109698.
[16] D. Pathania, R. Katwal, G. Sharma, M. Naushad, M.R. Khan, H. Ala'a, Int. J. Biol. Macromol. 87 (2016) 366–374.
[17] H. Wan, S. Weng, L. Liang, Q. Lu, J. He, Food Chem. Toxicol. 49 (2011) 3031–3037.
[18] S. Nakagawa, K. Sakakibara, H. Gotoh, Dyes Pigments 124 (2016) 130–132.
[19] A. Tkaczyk, K. Mitrowska, A. Posyniak, Sci. Total Environ. 717 (2020), 137222.
[20] A. Stammati, C. Nebbia, I. De Angelis, A.G. Albo, M. Carletti, C. Rebecchi, F. Zampaglioni, M. Dacasto, Toxicol. in Vitro 19 (2005) 853–858.
[21] M. Kooravand, S. Asadpour, H. Haddadi, S. Farhadian, J. Hazard. Mater. 407 (2021), 124878.
[22] F. Ding, W. Liu, F. Liu, Z.-Y. Li, Y. Sun, J. Fluoresc. 19 (2009) 783–791.
[23] M. Patra, C. Mukhopadhyay, A. Chakrabarti, RSC Adv. 5 (2015) 91166–91176.
[24] J.J. Weber, M.M. Kashipathy, K.P. Battaile, E. Go, H. Desaire, M.R. Kanost, S. Lovell, M.J. Gorman, Protein Sci. 30 (2021) 408–422.
[25] Y. Ma, R.D. Specian, K.-Y. Yeh, M. Yeh, J. Rodriguez-Paris, J. Glass, Am. J. Physiol. Gastrointest. Liver Physiol. 283 (2002) G965–G974.
[26] D.M. Frazer, G.J. Anderson, Biofactors 40 (2014) 206–214.
[27] B.S. Shamsian, N. Rezaei, M.T. Arzanian, S. Alavi, O. Khojasteh, A. Eghbali, Pediatr. Hematol. Oncol. 26 (2009) 356–362.
[28] F. Hashemi-Shahraki, B. Shareghi, S. Farhadian, Int. J. Biol. Macromol. 165 (2020) 1842–1851.
[29] S. Farhadian, B. Shareghi, S. Asgharzadeh, M. Rajabi, H. Asadi, J. Mol. Liq. 289 (2019) 1–10, 111111.
[30] S.M. Kelly, N.C. Price, Current protein and peptide science 1 (2000) 349–384.
[31] S. Asgharzadeh, B. Shareghi, S. Farhadian, Int. J. Biol. Macromol. 131 (2019) 548–556.
[32] S. Asgharzadeh, B. Shareghi, S. Farhadian, F. Tirgir, J. Mol. Liq. 280 (2019) 79–86.
[33] D.-L. Ma, D.S.-H. Chan, C.-H. Leung, Chem. Sci. 2 (2011) 1656–1665.
[34] C. Gao, Q. Shen, P. Tang, Y. Cao, H. Lin, B. Li, P. Sun, B. Bao, W. Wu, Molecules 26 (2021) 1816.
[35] T. Dutta, N. Baildya, A.A. Khan, N.N. Ghosh, Netw.Model.Anal.Health Inform. Bioinforma. 10 (2021) 1–11.
[36] S. Quazi T. Golani N. Akhtar C.E. Thomas Z. Haider bioRxiv, (2021).
[37] A. Lupia, S. Mimmi, E. Iaccino, D. Maisano, F. Moraca, C. Talarico, E. Vecchio, G. Fiume, F. Ortuso, G. Scala, Eur. J. Med. Chem. 185 (2020), 111838.
[38] T. Makarewicz R. Kaźmierkiewicz in, ACS Publications, 2013.
[39] L. Xing, X. Zheng, W. Sun, H. Yuan, L. Hu, Z. Yan, Spectrochim. Acta A Mol. Biomol. Spectrosc. 203 (2018) 455–460.
[40] T. Ahmed, M. Noman, J. Luo, S. Muhammad, M. Shahid, M.A. Ali, M. Zhang, B. Li, Int. J. Biol. Macromol. 168 (2021) 834–845.
[41] F. Heibati-Goojani, S. Farhadian, B. Shareghi, F.H. Shahraki, E. Ziaee, J. Mol. Struct. 1242 (2021) 1–12, 130702.
[42] F. Hashemi-Shahraki, B. Shareghi, S. Farhadian, J. Mol. Liq. 341 (2021), 117317.
[43] F. Heibati-Goojani, S. Farhadian, B. Shareghi, F.H. Shahraki, E. Ziaee, J. Mol. Struct. 1242 (2021), 130702.
[44] R. Eslami-Farsani, B. Shareghi, S. Farhadian, L. Momeni, Int. J. Biol. Macromol. 159 (2020) 433–443.
[45] M. Thirunavukkarasu, G. Balaji, S. Muthu, B.R. Raajaraman, P. Ramesh, Chem. Data Collect. 31 (2021), 100622.
[46] S.-R. Yan, M.M. Foroughi, M. Safaei, S. Jahani, N. Ebrahimpour, F. Borhani, N.R. Z. Baravati, Z. Aramesh-Boroujeni, L.K. Foong, Int. J. Biol. Macromol. 155 (2020) 184–207.
[47] M. Zhu, L. Wang, Y. Wang, J. Zhou, J. Ding, W. Li, Y. Xin, S. Fan, Z. Wang, Y. Wang, Int. J. Environ. Res. Public Health 15 (2018) 116.
[48] O.F. Sarioglu, A. Ozdemir, K. Karaboduk, T. Tekinay, J. Trace Elem. Med. Biol. 29 (2015) 111–115.
[49] D.A. Gacek, A. Betke, J. Nowak, H. Lokstein, P.J. Walla, Phys. Chem. Chem. Phys. 23 (2021) 8731–8738.
[50] L. Momeni, B. Shareghi, S. Farhadian, F. Raisi, J. Mol. Liq. 292 (2019), 111389.
[51] M. Mohammadi, B. Shareghi, A. Akbar Saboury, S. Farhadian, J. Biomol. Struct. Dyn. 38 (2020) 101–113.
[52] R. Assaran Darban, B. Shareghi, A. Asoodeh, J. Chamani, J. Biomol. Struct. Dyn. 35 (2017) 3648–3662.
[53] Y. Li, L. Yao, L. Zhang, Y. Zhang, T. Zheng, L. Liu, L. Zhang, Food Chem. 355 (2021), 129479.
[54] W. Cheng, J. Ma, S. Wang, R. Lou, S. Wu, J. He, H. Kang, L. Liu, F. Xiao, LWT 146 (2021), 111455.
[55] O. Mazuryk, K. Kurpiewska, K. Lewiński, G. Stochel, M. Brindell, J. Inorg. Biochem. 116 (2012) 11–18.
[56] F. Jafari, S. Samadi, A. Nowroozi, K. Sadrjavadi, S. Moradi, M.R. Ashrafi-Kooshk, M. Shahlaei, J. Biomol. Struct. Dyn. 36 (2018) 1490–1510.
[57] K. Fenner, G. Reynolds, S. Basu, Spectrochim. Acta A Mol. Biomol. Spectrosc. 239 (2020), 118473.
[58] V. Povedailo, B. Ronishenko, V. Stepuro, D. Tsybulsky, V. Shmanai, D. Yakovlev, J. Appl. Spectrosc. 85 (2018) 605–610.
[59] V. Koppal, R. Melavanki, R. Kusanur, N. Patil, J. Fluoresc. 31 (2021) 393–400.
[60] D. Meng, H. Zhou, J. Xu, S. Zhang, Chem. Phys. 546 (2021), 111182.
[61] S. Sarzehi, J. Chamani, Int. J. Biol. Macromol. 47 (2010) 558–569.
[62] S. Asadpour, Z. Aramesh-Boroujeni, S. Jahani, RSC Adv. 10 (2020) 31979–31990.
[63] N. Farajzadeh-Dehkordi, S. Farhadian, Z. Zahraei, N. Gholamian-Dehkordi, B. Shareghi, J. Mol. Liq. 327 (2021), 114835.
[64] E. Raeessi-babaheydari, S. Farhadian, B. Shareghi, J. Mol. Liq. 326 (2021), 115196.
[65] S. Sadeghi-Kaji, B. Shareghi, A.A. Saboury, S. Farhadian, Int. J. Biol. Macromol. 146 (2020) 687–691.
[66] H. Jafari-Arvari, S.S. Saei-Dehkordi, S. Farhadian, J. Mol. Liq. 339 (2021), 116715.
[67] S. Ren, M.M. Giusti, Foods 10 (2021) 310.
[68] H.A. Shilajyan, K.R. Grigoryan, Monatsh. Chem.Chem. Mon. 151 (2020) 135–139.
[69] Z. Asemi-Esfahani, B. Shareghi, S. Farhadian, L. Momeni, J. Mol. Liq. 332 (2021), 115846.
[70] R. Eslami-Farsani, B. Shareghi, S. Farhadian, L. Momeni, J. Biomol. Struct. Dyn. (2020) 1–12.
[71] N.N. Condurache, I. Aprodu, L. Grigore-Gurgu, B.A. Petre, E. Enachi, G. Râpeanu, G.E. Bahrim, N. Stănciuc, Food Chem. 318 (2020), 126508.
[72] A.F.C. Pacheco, N.M. Nunes, H.M.C. de Paula, Y.L. Coelho, L.H.M. da Silva, M. S. Pinto, A.C. dos Santos Pires, Int. Dairy J. 108 (2020), 104728.
[73] X. Li, H. Ji, Y. Bai, Z. Jin, Int. J. Biol. Macromol. 168 (2021) 640–648.
[74] S. Li, Z. Peng, R.M. Leblanc, Anal. Chem. 87 (2015) 6455–6459.
[75] A. Micsonai, É. Bulyáki, J. Kardos, BeStSel: from secondary structure analysis to protein fold prediction by circular dichroism spectroscopy, in: Structural Genomics, Springer, 2021, pp. 175–189.
[76] M. Mohammadi, B. Shareghi, S. Farhadian, A.A. Saboury, J. Mol. Liq. 330 (2021), 115710.
[77] S.-B. Kou, Z.-Y. Lin, B.-L. Wang, J.-H. Shi, Y.-X. Liu, J. Mol. Struct. 1224 (2021), 129024.
[78] J.L. Araújo, A. de Oliveira Sousa, G.T. Santos, L.A. de Sousa, Acta Sci.Anat. 1 (2021) 25–26.
[79] T.A. Wani, N. Alsaif, M.M. Alanazi, A.H. Bakheit, S. Zargar, M.A. Bhat, Eur. J. Pharm. Sci. 158 (2021), 105686.
[80] A. Sadaf, S. Kim, H.E. Bae, H. Wang, A. Nygaard, Y. Uegaki, Y. Du, C.F. Munk, S. Katsube, J. Bae, Acta Biomater. 128 (2021) 393–407.
[81] S. Jawalkar, S. Nataraj, A. Raghu, T. Aminabhavi, J. Appl. Polym. Sci. 108 (2008) 3572–3576.
[82] A. Raghu, G. Gadaginamath, S. Jawalkar, S. Halligudi, T. Aminabhavi, J. Polym. Sci. A Polym. Chem. 44 (2006) 6032–6046.
[83] M. Sargolzaei, J. Mol. Graph. Model. 103 (2021), 107803.
[84] T. Fukutani, K. Miyazawa, S. Iwata, H. Satoh, Bull. Chem. Soc. Jpn. 94 (2021) 655–665.
[85] S. Dong, S. Luo, K. Huang, X. Zhao, L. Duan, H. Li, Mol. Phys. 119 (2021), e1874558.
[86] E. Yamamoto, T. Akimoto, A. Mitsutake, R. Metzler, Phys. Rev. Lett. 126 (2021), 128101.

[87] S.A.H. Abdi, A. Alzahrani, M. Asad, A. Alquraini, A.I. Alghamdi, S.F. Sayed, J. Appl. Toxicol. 41 (2021) 1649–1659.
[88] T. Aslan, A. Yenenler-Kutlu, U. Gerlevik, A.Ç. Aktuğlu Zeybek, E. Kıykım, O. U. Sezerman, N. Birgul Iyison, J. Biomol. Struct. Dyn. (2021) 1–12.
[89] L. Zhang, P. Wang, Z. Yang, F. Du, Z. Li, C. Wu, A. Fang, X. Xu, G. Zhou, Food Hydrocoll. 101 (2020), 105455.
[90] H. Chen, A.Z. Panagiotopoulos, Langmuir 35 (2019) 2443–2450.
[91] V. Ferraro, A.R. Madureira, P. Fonte, B. Sarmento, A.M. Gomes, M.E. Pintado, RSC Adv. 5 (2015) 88529–88538.